Chemistry Europe
European Chemical Societies Publishing

WILEY VCH

Excellence in Chemistry Research

Announcing our new flagship journal

- Gold Open Access
- Publishing charges waived
- Preprints welcome
- Edited by active scientists

Meet the Editors of *ChemistryEurope*

Luisa De Cola
Università degli Studi di Milano Statale, Italy

Ive Hermans
University of Wisconsin-Madison, USA

Ken Tanaka
Tokyo Institute of Technology, Japan

ChemistrySelect

Research Article
doi.org/10.1002/slct.202104323

Chemistry Europe
European Chemical Societies Publishing

www.chemistryselect.org

Materials Science inc. Nanomaterials & Polymers

Superior CdSe/ZnS@Fe_2O_3 Yolk-Shell Nanoparticles as Optically Active MRI** Contrast Agents

Derya D. Ekici[a] and Evren Mutlugun*[b, c]

We have developed a robust synthesis methodology for quantum dots (QDs) nanoparticles with magnetic properties designed for biomodal imaging. These nanocrsytlas consists of a semiconductor quantum dot core with engineered fluorescence, which is located in a paramagnetic iron oxide shell that acts as a magnetic resonance imaging (MRI) contrast agent. Yolk-shell CdSe/ZnS@Fe_2O_3 nanoparticles (NPs) are synthesized via sonochemical decomposition of iron pentacarbonyl ($Fe(CO)_5$) using the oleylamine (OAm) as the ligand. The sonochemical synthesis method of magnetic fluorescent NPs that can be used as MRI contrast agents provided advantages such as improved quantum efficiency and homogeneous size distributions. It has been determined that the luminescence efficiency of quantum dots decreases in coatings that can be made at high temperatures by thermal decomposition. In order to eliminate the disadvantage of elevated temperatures, the sonochemical decomposition method, which allows coating at low temperatures, has been used. With this method, yolk-shell (CdSe/ZnS@Fe_2O_3) nanoparticles were produced with high photoluminescence quantum efficiency and homogeneous size distributions. The synthesis magnetic fluorescent NPs optimized was determined to have the injection temperature of $Fe(CO)_5$ at 60 ° C, $Fe(CO)_5$/CdSe@ZnS ratio 0.7, OAm/$Fe(CO)_5$ volume ratio 1.43 with an oxidation time 5 min. Under these conditions, the quantum efficiency was found to be 78%, nanoparticle sizes between 11–14 nm and r_1 value was 0.199, r_2 value was 0.518 in MRI analysis. These optically active magnetic fluorescent nanoparticles as positive contrast agents (T1 weighted) are predicted to pave the way for the future of advanced bioimaging systems.

1. Introduction

Colloidal quantum dots (QDs) have attracted much attention in the last few decades thanks to their optoelectronic properties. Chemically stable, size-controlled nanocrystals with narrow emission profiles offer distinct advantages over other fluorescent markers such as proteins or dyes. QDs can be 20 times brighter and 100 times more stable, making them ideal for imaging, ultra-sensitive detection and labeling applications.[1] Also, QDs allow for modification of functional groups on their surface. This allows QDs to be usable suitable for various applications. Amongst the common applications of those QDs is detection and bioimaging, which show considerable advantages over existing biomedical detection systems to foster sensitivity and selectivity.[2] The various spectral range of multicomponent alloy QDs are the most widely researched given that many reaction parameters can be controlled.[3] The utilization of chemical functionalization at QD the interfaces is benefitial for the aqueous medium, that is necessary for bioimaging applications.[4] The carboxyl functional groups on the surface of QDs makes them available to be conjugated to free amines on biomolecules through amide bond formation.[5] These protocols are mostly on the generation of new synthesis recipes for QDs that provide a customizable hydrophilic structure, chemical and photostability and functionalization. The surface modification should not only be able to prevent degredation, but also provide solubility at reasonable ionic strengths and should also allow attaching additional functional groups through ligand chemistry at the surface. In addition, the surface modification also needs to avoid carrier traps. This type of surface modification is particularly important for biodiagnostic and biological imaging studies.[4] Oleylamine (OAm) is a very common organic solvent that is liquid at room temperature and therefore benefitial for the post synthesis excess ligand removal procedures.[6] It is assumed that the formation of core-shell/yolk-shell particles is through the utilization of the amine groups of the OAm.[7] OAm has a double bond in the middle of the chain which is a better closing ligand due to its long carbon chain and double bond facilitating dissolution.[8] The system can be activated or passivated depending on the density of ligands on the surface of the QDs. When the surface of QDs is activated, functional groups or composite nanostructures can be created on the surface.[9]

On the other hand, the production of monodisperse magnetic MNPs has attracted great attention recently, owing their chemical stability and biocompatibility. They are widely used in optical and magnetic applications in heterostructures,

[a] *Dr. D. D. Ekici*
Department of Materials Science and Nanotechnology Engineering, Abdullah Gul University, Kayseri, Turkey TR-38039
[b] *Prof. E. Mutlugun*
Department of Electrical-Electronics Engineering, Abdullah Gul University, Kayseri, Turkey TR-38039
E-mail: evren.mutlugun@agu.edu.tr
[c] *Prof. E. Mutlugun*
UNAM – Institute of Materials Science and Nanotechnology, Bilkent University, Ankara 06800, Turkey

[**] *MRI: Magnetic resonance imaging*

Supporting information for this article is available on the WWW under https://doi.org/10.1002/slct.202104323

biomedicine and catalysts, as well as unique structures as dual imaging probes for MRI and optical imaging.[10] The study of iron as a magnetic material recently have gained importance, for their use in biomedical applications, based on thesi high specific heat, high strength and their approval by the Food and Drug Association. Based on this, iron holds great potential for targeted drug delivery and MRI.[11]

Regarding MRI applications, paramagnetic nanomaterials offer advantages over conventional coordination complexes. As an example, their size, shape and composition can be engieered easily. The magnetic properties can be manipulated by geometric local density effects, which yield significantly higher T1 and/or T2 relaxant values. In order to further reduce the toxicity of free metal ions and develop contrast agents that can cross the blood brain barrier, research on paramagnetic contrast agents has recently focused on the development of nanostructured materials.[12] Multifunctional magnetic NPs have already been shown for MRI imaging applications. MRI technology allows for creation of high-quality images, but further development of magnetic contrast agents is required.[13] Imran et al. studied the dispersion of iron oxide nanoparticles in a carrier medium. Ferrofluids were synthesized by using different oil types or mixtures. The thermal conductivity and stability of these synthesized ferrofluids were increased. It has been reported that these ferrofluids can also be used in health fields such as MRI and magnetic induced hyperthermia.[14,15,16] Iron-based nanomedicine, which has been widely confirmed in the medical world as the most successful inorganic metal ever created in the context of nanomedicine, has recently concentrated on the utilization of iron-based MRI as a positive contrast agent. Since the positive contrast agents typically used in clinical practice are Gd complexes that pose health risks to patients, some authors have taken an interest in the use of iron oxide NPs as T1 contrast agents. Because of its magnetic characteristics, biocompatibility, and targeting potential, iron oxide NPs have been studied for decades. Iron oxide NPs are generally negative contrast agents, in contrast to the Gd-based contrast agents now in use.[12] Negative imaging agents, that is, T2-weighted MRI appear dark and create confusion. Also, when imaging tumors, it is difficult to distinguish images between metal deposits and signals from calcification. As a result, the researchers directed their efforts to design a promising positive contrast agent, namely super paramagnetic ıron oxide NPs based on ultra-small monodisperse magnetite (Fe_3O_4) that can measure T1-weighted. However, there is still a clear challenge to obtain excellent T1-weighted MRI contrast agents with good biocompatibility, sensitivity, and early diagnosis of diseases.[17] Additionally, when nanoparticles are extremely tiny in size, thermal energy may easily translate their magnetism. Their actions exhibit paramagnetic behavior in this situation.[12]

It is known that the thermal decomposition of $Fe(CO)_5$ used in the production of advanced composite nanostructures is one of the most successful and frequently used techniques.[11] Generally, the coating can be achieved by temperature change.[18] $Fe(CO)_5$ and oleyamine (OAm) reaction is in the group containing less CO. It is well known that $Fe(CO)_5$ in combination with various ligands forms an intermediate. OAm can work as a surfactant even after the reaction's precursor has broken down in situations where certain CO ligands are anticipated to be replaced by it. As a result, it can protect the particle against oxidation.[19] Metal oxides generally exhibit greater biocompatibility than base metals. After passive oxidation, nanoparticles coated with an oxide shell maintain a stable core. Also, since it is ferromagnetic, the application of a metal oxide shell increases the magnetic susceptibility of non-magnetic materials.[11]

Yolk or core / shell nanocomposite is regarded as a core nanoparticle totally encapsulated by a shell coating. Under the shell, the surface of the core is entirely encased, which hinders the material's characteristics.. OAm coated QD nanoparticles are first synthesized separately. These QD-OAm nanoparticles are then reacted with Fe complexes while the newly formed FexOy nanoparticle is deposited on the QD surface.[9] The resultant NPs are highly magnetic materials for applications requiring minimal toxicity and biocompatibility since the ensuing heterostructures have been proven to shield oxidatively unstable nuclei.[11] Kim and Song created a hybrid system with Pd and Fe3O4 components, and they used a combination of capping agents, OAm and oleic acid, to carefully regulate the nucleation and development of the Fe component on the Pd surface (OA). The egg yolk shell, irregular core-shell, and dumbbell-shaped nanoparticles were the first Pd-Fe3O4 structures to form following oxidation. The mean crystal field size of Fe3O4 and the area of Pd that was exposed to the outside were concurrently altered by the change in morphology, which had an immediate impact on the materials' respective catalytic and magnetic capabilities..[20] Totipotential materials equipped with advantages in different aspects required the urgent need for effective solutions to the challenges and encouraged research into the design of multilayer heterogeneous structures. It is still under investigation to combine the advantages of various components in a single integrated material. The top priority is the synthesis technique. Due to the apparent polarity contrast between the solvent and the particles, these particles do not disperse well in standard solvents. Even if the additional additive can reduce the distance to some amount, there is still insufficient bonding power between the two materials.[21]

Due to the optical and chemical advantages of NPs, QD-based nanotechnology can help create a biomedical imaging platform for studying cancer cell behavior. The rapid development of immunohistochemistry (IHC) has led it to become an important complementary tool for diagnosis and research in a clinicopathological setting. High sensitivity and specificity in addition to an imaging system are key factors as the technology underlying IHC involves antigen-inter antibody interactions. The development of semiconductor QDs will lead to the creation of an interdisciplinary field that includes bioassays and bio-imaging technologies. QDs combined to materials with similar imaging and therapeutic function produce a variety of biological functional probes that can be used simultaneously for tumor molecular imaging and targeted therapy.[22] Most studies suffer from a number of the drawbacks of high temperature production, such as limited amplification or connecting issues with single-mode fibers, despite showing

the immense potential of QD-based fibers. The effectiveness of QD-based fiber amplifiers at high temperatures has not been extensively studied. This is problematic because it's crucial to have good thermal stability in a range of settings. Although this synthesis appears promising, applications for this structure are severely hampered by the low thermal stability associated with QDs, which causes amplification signals to be lost at higher temperatures. However, as anticipated, the PL density of OLAm-QDs drops with heating and does not increase throughout the cooling phase..[23]

Till date; Chen et al presented colloidal superstructures consisting of tightly packed magnetic nanoparticle cores completely surrounded by a shell of fluorescent QDs. This silica-coated core-shell structure has been reported as approximately 100 nm.[24] Feld et. al. published research on iron oxide covered with polystyrene and quantum dot/quantum rod. They claimed that nanoparticles with tunable diameters ranging from 74 to 150 nm were generated, and that the fluorescence and magnetism of the individual components were retained. It has been reported that these hybrid structures developed are also suitable for surface modifications, but their large size may limit the visualization of the intracellular environment. Size was shown to be a crucial factor that determines how precisely the nanomaterial will be integrated into the cell, along with its impact on cellular absorption efficiency and kinetics, subcellular distribution, saturation concentrations, and toxicity.[25] To overcome the drawback, Pahari et. al. presented a general strategy and a promising new hybrid structure comprising a fluorescent QDs core encapsulated in a hollow magnetic shell providing MRI contrast agent (CdSe@CdS@Hollow-Fe_2O_3). In this study carried, ultra-small magneto-fluorescent nanoparticles (15 nm hydrodynamic size) were produced and it was reported that these nanoparticles have high quantum yields. Thermal decomposition was used in the study.[26] However, the effect of the temperature used on the quantum yield has not been specified.

Reaz et. al. (2020) created ZnO/iron oxide core-shell nanostructures with controllable magnetic characteristics using a low-cost sonochemical production method. In the thin (0.5–3nm) crust area of atomic dimensions, subtle structural differences between maghemite (-Fe_2O_3) and its reduced form magnetite (Fe3O4) were identified. By fusing solid state chemistry with nanotechnology to create multifunctional core-shell oxide nanomaterials from the ZnO core of high luminescence, they have demonstrated a new technique for creating novel nanomaterials.In this way, they paved the way for coating at low temperatures.[27]

In this study, in order to account for a solution in the synthesis of optically active magnetic nanoparticles, useful designs of QD-Fe_xO_y nanocomposite materials are investigated. In order to eliminate the disadvantages caused by high temperatures, synthesis was carried out by sonochemical method instead of thermal decomposition. To enhance their qualities, the QD and Fe_xO_y components' size and thickness can be changed.. As control parameters, ambient temperature, concentration of components and sonication rate were investigated in detail. The surface nature of QD-Fe_xO_y nanocomposites can be adjusted by bonding and functionalizing different chemical parts.

2. Results and Discussion

Quantum yield change with $Fe(CO)_5$ concentration and oxidation time of magnetic fluorescent NPs prepared at different temperatures: It is known that there is irreversible loss of the quantum yield of CdSe/ZnS@Fe_2O_3 produced at high temperatures in QD coating with OAm. In order to eliminate this bottleneck and show that the quantum efficiency decreases at high temperatures, magnetic fluorescent NPs synthesis was carried out at different temperatures. Figure 1, demonstrates the quantum yields of magnetic fluorescent NPs synthesized at 60, 80, 100 and 120 °C injection temperature and 70% sonication rate. As shown in Figure 1., it is clearly seen that as the temperature decreases, the photoluminescence efficiency of magnetic fluorescent NPs produced by sonochemical method increases.

After the iron carbonyl injection at 120 °C, the efficiency of quantum dots with magnetic properties produced by sonochemical decomposition was found to be low. The temperature affects the structure negatively. The irreversible loss of quantum dot efficiency, since the coating cannot be properly made, ıs subject. It is thought that not only Fe surface but also the quantum dot surface is oxidized during oxidation. It has been determined that these negativities are related to high temperature. During the synthesis phase, the $Fe(CO)_5$ injection temperature was decreased and the reaction continued. With the initial $Fe(CO)_5$/CdSe@ZnS weight ratio is 0.7, CdSe/ZnS@Fe yield of 11.9 was obtained at 100 °C injection temperature. Maximum efficiency was reached in the weight ratio of $Fe(CO)_5$/CdSe@ZnS of 0.7 at the 5th minute of oxidation. At the 5th minute of oxidation $Fe(CO)_5$/CdSe@ZnS weight ratio is 0.7, magnetic fluorescent NPs quantum yield of 40.4 was obtained. When oxidation continues, the quantum dot nucleus is degraded, thus photoluminescence efficiency decreases. The maximum quantum yields reached during oxidation of the magnetic NPs produced at 100 °C injection temperature did not approach the bare quantum dot quantum yields. With the initial $Fe(CO)_5$/CdSe@ZnS weight ratio of 0.7, CdSe/ZnS@Fe quantum yield of 22.6% were obtained at 80 °C injection temperature. Maximum efficiency was reached by the weight ratio of $Fe(CO)_5$/CdSe @ ZnS of 0.7 at the 15th minute of oxidation, At the 15th minute of oxidation $Fe(CO)_5$/CdSe@ZnS weight ratio of 0.7, respectively; magnetic fluorescent NPs quantum yield of 33.9 were obtained. In order to increase the photoluminescence efficiency, lower temperature production was carried out. With the initial $Fe(CO)_5$/CdSe@ZnS weight ratio is 0.7, CdSe/ZnS@Fe yield of 28.9 was obtained at 60 °C injection temperature. Maximum efficiency was reached in the weight ratio of $Fe(CO)_5$/CdSe @ ZnS of 0.7 at the 5th minute of oxidation. At the 5th minute of oxidation $Fe(CO)_5$/CdSe@ZnS weight ratio is 0.7, magnetic fluorescent NPs quantum yield of 67.5 was obtained.

In order to examine the effect of $Fe(CO)_5$ different concentrations against the quantum yields of magnetic nano-

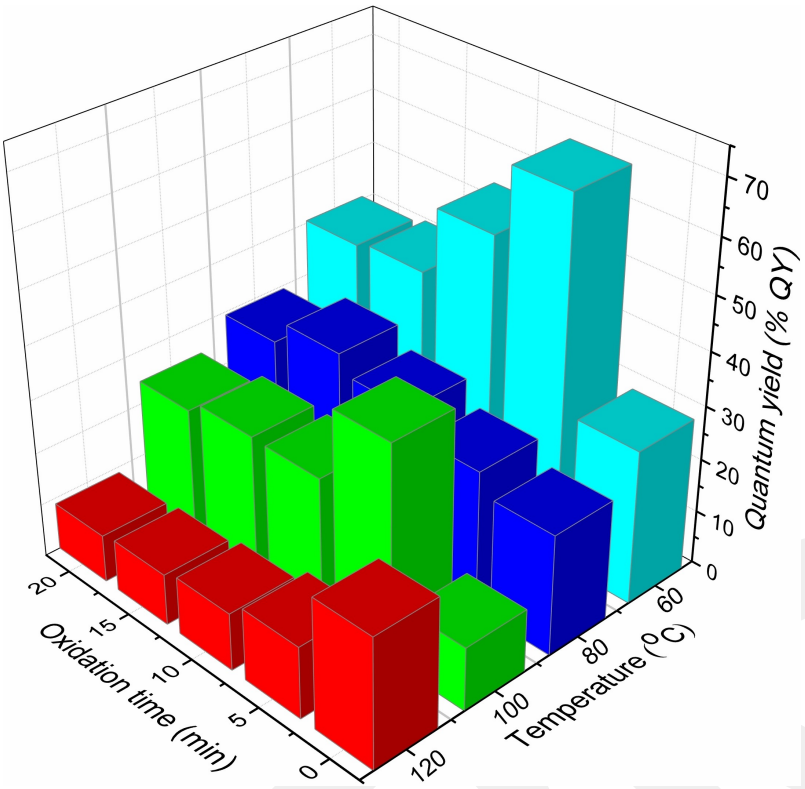

Figure 1. The effect of temperature change and oxidation time on the quantum yield of magnetic fluorescent NPs produced at $Fe(CO)_5$/CdSe@ZnS weight ratio of 0.7.

particles, production was carried out at an injection temperature of 60 °C. these values are shown in Figure 2. With the initial $Fe(CO)_5$/CdSe@ZnS weight ratio increasing from 0.5 to 0.8, respectively; CdSe/ZnS@Fe quantum yield of 36.47, 20.23, 28.87 and 28.79 were obtained. This binary system's relatively high fluorescent quantum efficiency decreased after coating, indicating that the gap between the iron oxide shell and the CdSe@ZnS core in nested morphology does not allow for the energy or charge transfer between them. Nesting nanoparticles, often referred to as "yolk-shell" formations, form when the first metallic particle to be oxidized encloses a different substance, as is the case in this instance.[26]

As a consequence, the CdSe@ZnS was enclosed in a hollow Fe2O3 iron oxide shell created by the controlled oxidation of the iron. It has been determined that oxidation smoothens the surface and increases the quantum yield of photoluminescence by reducing the space between the shell and the core. Maximum efficiency was achieved by the weight ratio of $Fe(CO)_5$/CdSe@ZnS was 0.5 at the 15th minute of oxidation. At the 15th minute of oxidation $Fe(CO)_5$/CdSe@ZnS weight ratio of 0.5, magnetic fluorescent NPs quantum yield of 41.1 were obtained. Maximum efficiency was reached by the weight ratio of $Fe(CO)_5$/CdSe@ZnS was 0.6 and 0.8 at the 10th minute of oxidation. At the 10th minute of oxidation $Fe(CO)_5$/CdSe@ZnS weight ratio of 0.6 and 0.8, respectively; magnetic fluorescent NPs quantum yield of 40.5 and 34.9 were obtained. Maximum efficiency was reached by the weight ratio of $Fe(CO)_5$/CdSe@ZnS was 0.7 at the 5th minute of oxidation. At the 5th minute of oxidation weight ratio of 0.7, magnetic fluorescent NPs quantum yield of 67.46 were obtained. As in all temperature conditions, it has been observed that the magnetic fluorescent NPs collapse is unstable when $Fe(CO)_5$/CdSe@ZnS weight ratio of 0.8. Again, when $Fe(CO)_5$/CdSe@ZnS weight ratio is 0.5 at all temperature conditions, it has been determined that the losses after magnetic separation are high in which not all QDs are covered. It was found that the highest photoluminescence efficiency was reached after oxidation when $Fe(CO)_5$/CdSe@ZnS weight ratio was 0.7 in weight and the magnetic property was good at this value.

The most important feature of the sonochemical method is that it allows for achieving more homogeneous and smaller size distributions. At the same time, the thickness of the iron layer coated with the sonication speed can be changed. Therefore, the quantum efficiency can be increased. According to this prediction, the effect of sonication rate was investigated. As the sonication rate increased, the photoluminescence efficiency of magnetic fluorescent NPs increased due to the decrease in coating thickness and air bubbles. With sonication rate increasing from 70% to 90%, respectively; CdSe/ZnS@Fe yield of 28.87, 54.2 and 75.6 were obtained. For the synthesis carried out at 70% and 80% sonication speed, it was observed that as the oxidation time increased, the magnetic fluorescent NPs yields first increased and then decreased. This is due to the oxidation of the iron on its surface first and then the oxidation

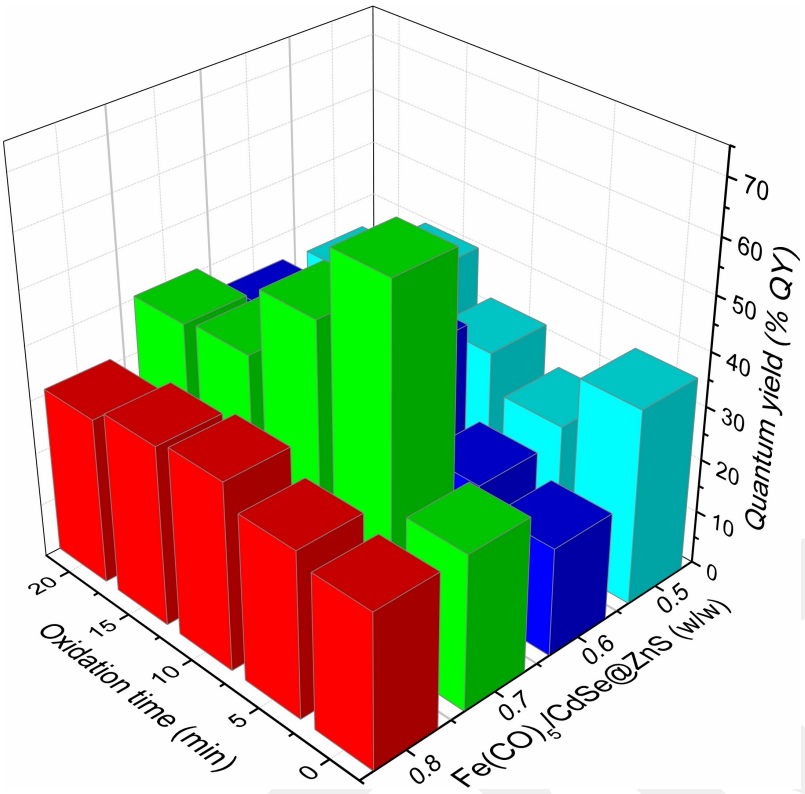

Figure 2. The effect of $Fe(CO)_5$ concentration and oxidation time on the quantum yield of magnetic fluorescent NPs produced at 60 °C injection temperature.

of the QDs. Therefore, oxidation of the material for 5 minutes will be sufficient for the system. For the 90% sonication rate, the coating is very thin and the air bubbles between the coating and the QDs are so small that the QDs are damaged when oxidizing begins. Photoluminescence efficiency of magnetic fluorescent NPs has decreased from the beginning to the end of oxidation. The highest magnetic fluorescent NPs efficiency was obtained at the production stage when 80% of the sonication rate and after 5 minutes of oxidation. The highest quantum yield was determined as 78.

When the size distributions of magnetic particles were examined by sonication speed and oxidation time, first increase and then decrease in the size of magnetic particles depending on the oxidation time were analyzed. this judgment was observed only at 90% sonication rate, first decrease then increase in the oxidation process. After 10 minutes of oxidation process, it was determined that the structure deteriorated and aggregated over time. When the size distributions are examined (Figure S-1), the sizes of magnetic nanoparticles vary between 10 nm and 14 nm.

Dimensional analysis of QDs and magnetic fluorescent NPs were performed to examine the numerical size analysis and dimensional differences. Size distribution analysis obtained from zeta sizer is shown in Figure 3(a). The dimensions of the magnetic nanoparticles at the highest photoluminescence efficiency were found to peak at 11 nm. It has been determined that the size distribution of QDs that do not have magnetic properties peaks at 8.5 nm. Hence the thickness of the iron oxide layer was determined to be around 2.5 nm. Figure 3(b) shows the TEM analysis image of magnetic fluorescent NPs. It was determined that there is a homogeneous size distribution in the TEM image.

The effect of OAm concentration on the photoluminescence efficiency of magnetic fluorescent NPs was investigated. Data are presented in Figure 4.

The quality of iron deposition on the surface and, consequently, the shape of the yolk-shell system were shown to be influenced by the capping ligand of the fluorescent QD core. Numerous capping ligands, such as trioctylphosphine oxide (TOPO), octadecyl ammine, and oleylamine, were investigated. Oleylaminecapped nanoparticles are reported to result in the highest quality structure.[24] It has been found that when the volume ratio of $OAm/Fe(CO)_5$ are 1.72 and 2, magnetic fluorescent NPs tend to collapse due to excess iron accumulation on the QDs surface. Therefore, the photoluminescence efficiency of magnetic fluorescent NPs with increased coating thickness decreased. The oxidation stage was not sufficient to increase these yields. When the volume ratios of $OAm/Fe(CO)_5$ are 0.86 and 1.14, it has been determined that iron accumulation on the QDs surface is not fully realized, since its magnetic properties are not sufficient. The optimum volume ratio of $OAm/Fe(CO)_5$ was determined to be 1.43. In this condition, magnetic fluorescent NPs work with maximum efficiency.

XRD and XPS Analysis: Structural characterization of the ultrafine coating of atomic sizes has not been easy with techniques such as XRD and XPS owing the the existence of

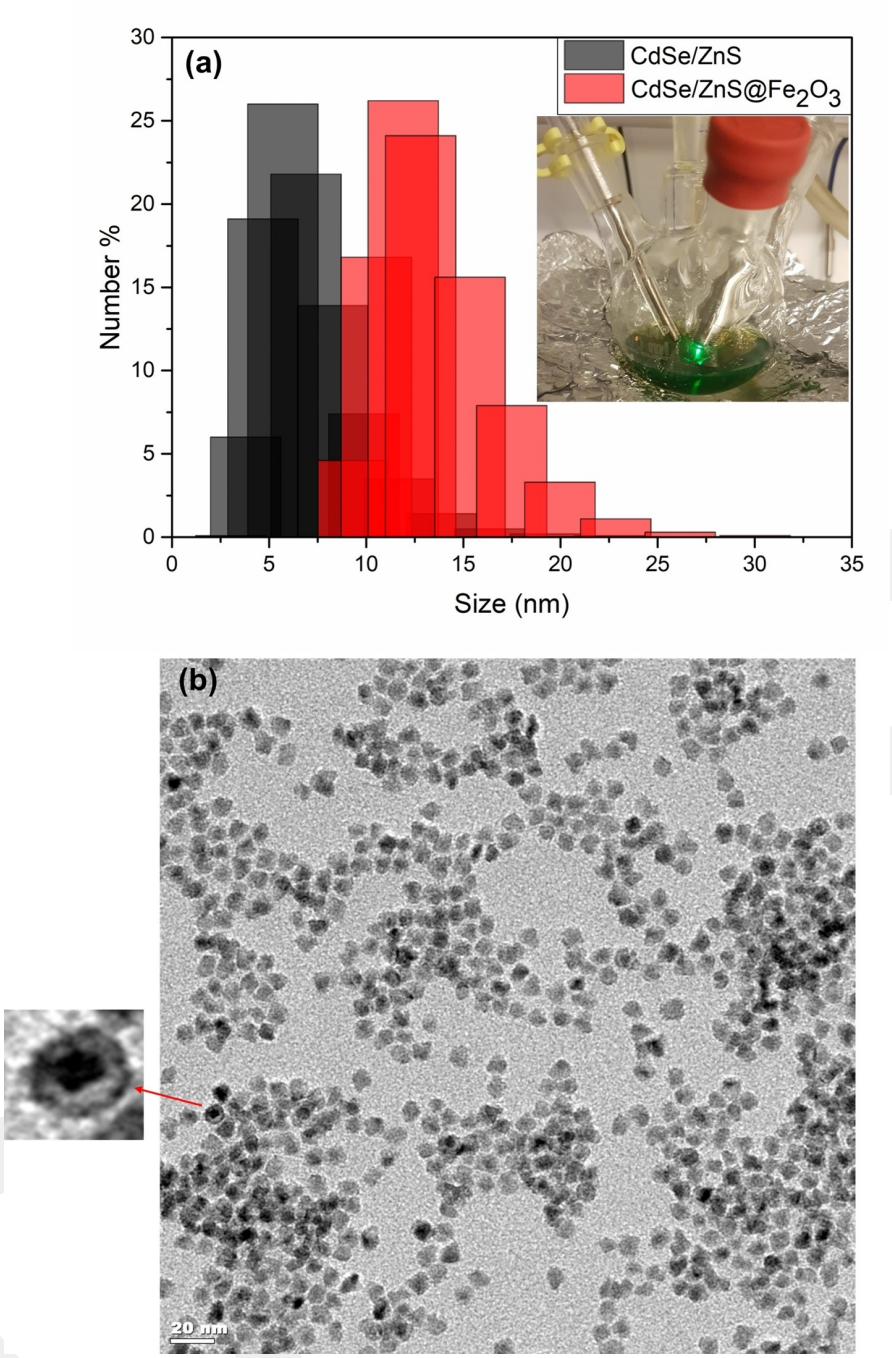

Figure 3. (a) Size distribution of QDs and magnetic fluorescent NPs by number (b) TEM images of magnetic fluorescent NPs.

nano-crystallites, and also due to the the relatively limited number (as low as 1–4%) of the shell phase atoms.[27]

XRD and XPS analyzes were performed to examine the differences in the structural analysis of the synthesized magnetic fluorescent NPs. X-ray diffraction (XRD) measurements were used to examine the crystal structure of CdSe/ZnS QDs. The XRD pattern of CdSe/ZnS (bulk CdSe (JCPDS No. No. 00-019-0191) and bulk ZnS (JCPDS No. 80-0020)) shows peaks at 28.49, 47.386 and 56.223 degrees corresponding to the lattice planes of (111), (220) and (311) (Figure 5a), respectively. The XRD peaks shrink as the thickness of the shell rises, showing that the QDs expand when ZnS shells form in CdSe nuclei in the zinc blade.[28]

In XRD, the shell thickness of the CdSe/ZnS coated iron oxide shell layer at the nano level (0.5-5 nm) could not be distinguished between these two phases. Hence, the iron oxide Shell layer was analyzed with the more sensitive XPS analysis. Given that XPS is a highly surface-sensitive technology, this is to be expected. In Figure 5(b) and 5(c), compares the XPS analysis of quantum dot and magnetic fluorescent NPs. When

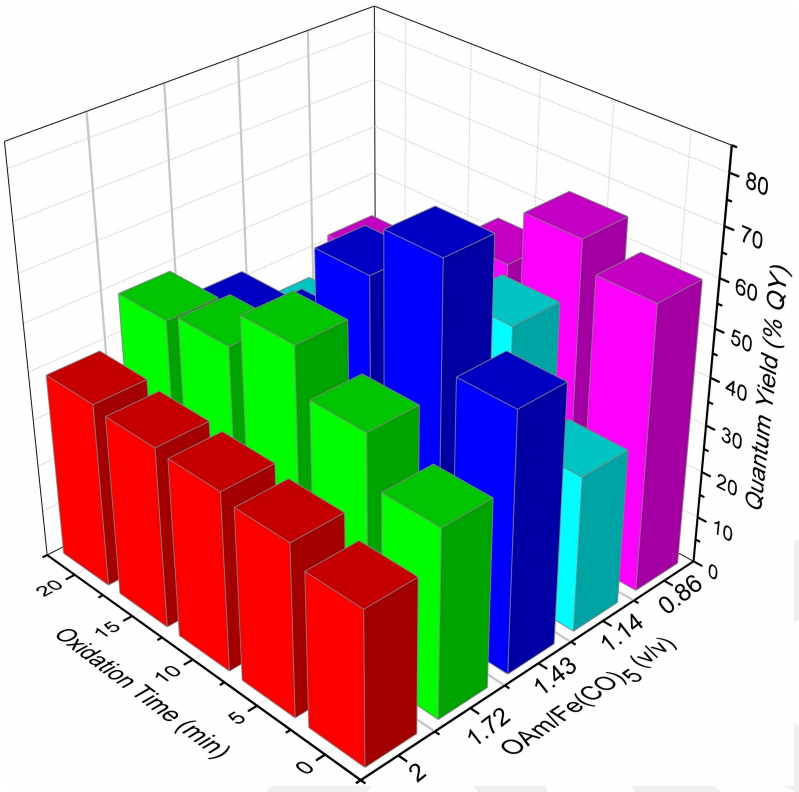

Figure 4. The effect of OAm concentration and oxidation time on the photoluminescence yield of magnetic fluorescent NPs produced at 60 °C injection temperature.

this figure is examined, the quantum dot shown with the red line (b) represents the magnetic fluorescent NPs shown with the blue line (c). We specified 6 peaks associated with CdSe/ZnS in the XPS model. When these peak values were examined, it was determined that Se3d (55.3 eV), S2 s (227.1 eV), C1s (286.08 eV), Cd3d (406.04 eV), O1s (532.87 eV) and Zn2p3 (1021.81 eV) structures. When the areas at these peak values are examined, the impurity phase is almost nonexistent. In the magnetic fluorescent NPs shown in blue, the same peaks were determined, as well as a different peak. The peak difference is visible on the blue line. this peak value started at 728 eV and ended at 704 eV. The peak value of this peak was determined to be 709.41 eV.

Peaks at 710.7, 719.6, 725.1 and 733.4 eV, respectively, are identified by the orbitals of Fe (2p 3/2, 2p 3/2 and 2p 1/2) and its satellite (2p 1/2). No satellites around 715 and 728 eV can confirm that there are no Fe (II) atoms on the surface. A high stoichiometric ratio between the O2 and Fe atoms is consistent with the O1s peak's high phase percentage. This demonstrates that maghemite, not magnetite, makes up the surface layer.[27]

In the light of this information, the presence of maghemite phase in the crust was detected in the sample shown with a blue line. The reason why the peak intensity is not high is that the thin iron oxide shell phase was designed in order not to prevent the radiation of the quantum dots. Therefore, there are difficulties in XRD and XPS measurements. In the figure, Fe 2p3/2, around 709.41 eV, indicates the presence of the high spin Fe (III) oxide phase (Y-Fe_2O_3). In summary, the Fe2p 3/2 peak at 709.41 eV firmly proves that the oxidized iron oxide phase is maghemite.

MRI Relaxivity Measurements: Superparamagnetic iron oxide (SPIO) and ultrafine superparamagnetic iron oxide are the two different forms of iron oxide contrast agents (USPIO). Iron oxide nanoparticle suspension colloids make up superparamagnetic contrast agents. These imaging-related nanostructures lessen the strength of T2 signals in tissues that take up the contrast agent. With the use of this approach, liver tumors have been successfully diagnosed. In clinical application, iron oxide is a common and distinctive nanoparticulate agent that allows for variations in the sizes and particle shapes of this category of contrast materials as well as the applied surface coating.Therefore, it is possible to make changes in the signals of these contrast agents with changes in the production method and surface modifications.[29] To improve visibility and magnetic resonance imaging, contrast chemicals can alter the signal intensity in various tissues. The modification of the longitudinal and transverse relaxation durations to produce disparities between neighboring tissues determines the efficacy of contrast agents with regard to various agent absorption. These alterations are classified as "positive," which denotes high signal intensity, or "negative," which denotes low signal intensity in T1 and T2-weighted images. This is why magnetic fluorescent NPs were first subjected to PEG binding before MRI analysis.[30] When interpreting magnetic properties, relaxation

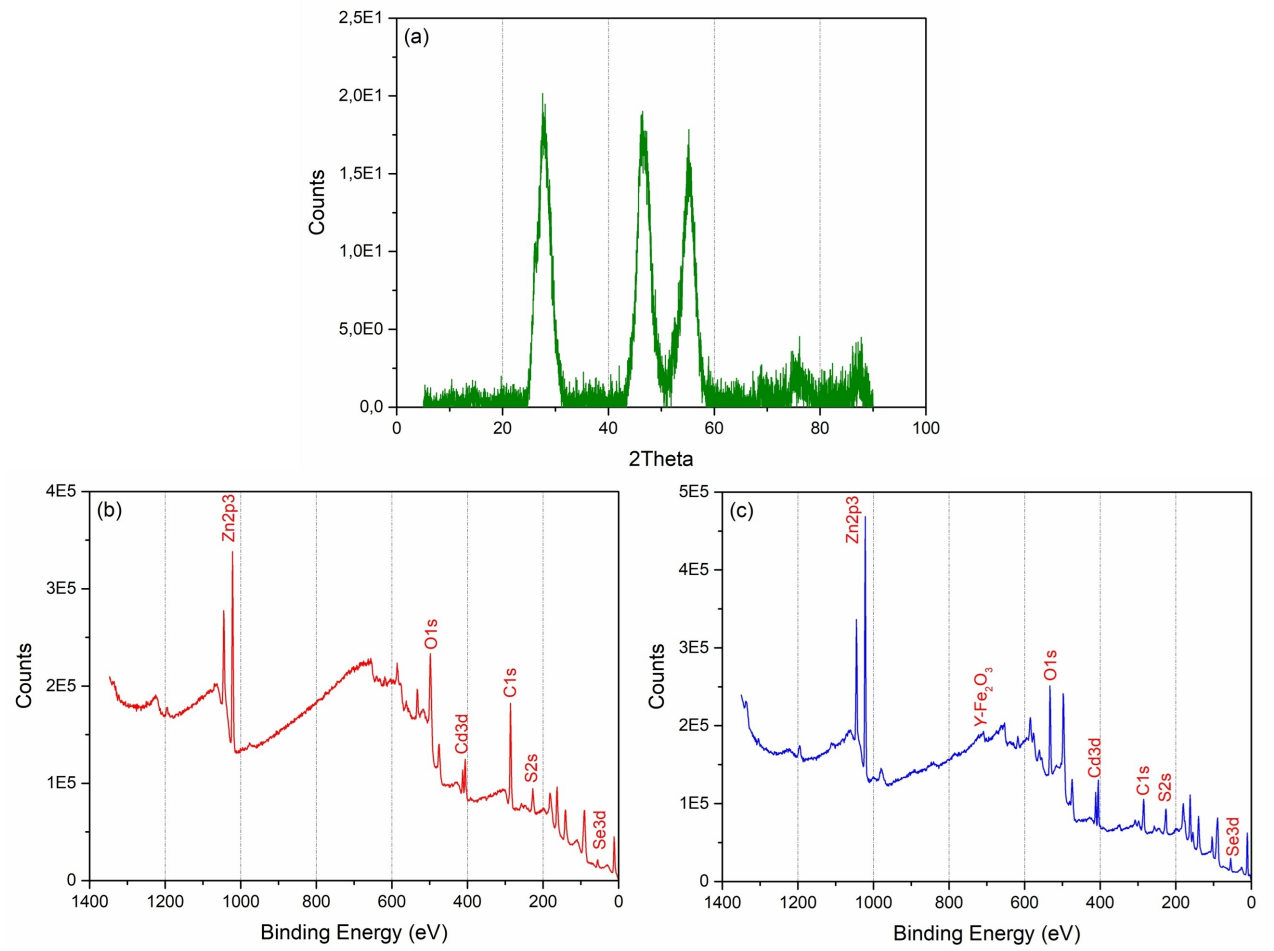

Figure 5. (a) Powder X-ray diffraction (XRD) patterns of green-emitting CdSe/ZnS (b)XPS analysis of green-emitting CdSe/ZnS quantum dot (c) XPS analysis of magnetic fluorescent NPs.

(r), particularly the ratio r_2 / r_1, which defines the potential to be a positive or negative contrast agent, is very important.[31] The r_2/r_1 ratio indicates whether a contrast agent is suitable for positive (T1) or negative (T2) contrast while defining the signal enhancement capabilities of that contrast agent. T2 contrast agents often have a higher r_2/r_1 ratio (>10) compared to T1 contrast agents, which typically have a lower r_2/r_1 ratio (<5).[12]

After being mixed with a pH 7.4 phosphate buffer and sonicated, it was observed that the large particles settled to the bottom and there were stable nanostructures on the upper part. this has caused minor errors in concentrations. but this did not affect the visibility of the structure very much. However, due to the high molecular weight of PEGlated nanoparticles, r_2 / r_1 values are high. These values decrease as lower molecular weight polymers are used during coating.[30] The initial concentration of all samples was 1 mM. They were transferred into smaller 1.5 mL containers and a dilution series (0.8, 0.4, 0.266, 0.2, 0.16, 0.133 Mm) was prepared. The sample was provided in solid form.

MRI analysis graphics are given in Figure 6(a) and 6(b). When analyzing MRI for magnetic fluorescent NPs, r_1 value was determined as 0.199 mM^{-1} s^{-1} and r_2 value as 0.518 mM^{-1} s^{-1}. When r_2/r_1 value is taken as reference, this value was determined as 2.60 and it was found to be in the positive contrast agent class.

Superparamagnetic agents belong to the group of negative contrast agents. These compounds can also become T1 agents depending on particle size and coating.[29] MRI images of nanoparticles are shown in Figure 6(c). In T1-weighted images, it was observed that the brightness of the nanomaterial increased as the concentration increased. The image power increases as the amount of material produced increases and then starts to saturate after 0.266 mM. It can be said that its visibility and brightness as a positive contrast agent at low concentrations are very good. The MRI results show that the synthesized CdSe/ZnS@Fe_2O_3 nanoparticles are a promising candidate for T1-weighted MRI contrast agent.

When the dimensions, XRD, XPS and MRI analyzes of these magnetic fluorescent NPs nanoparticles are examined, the structures are thought to be superparamagnetic structures.

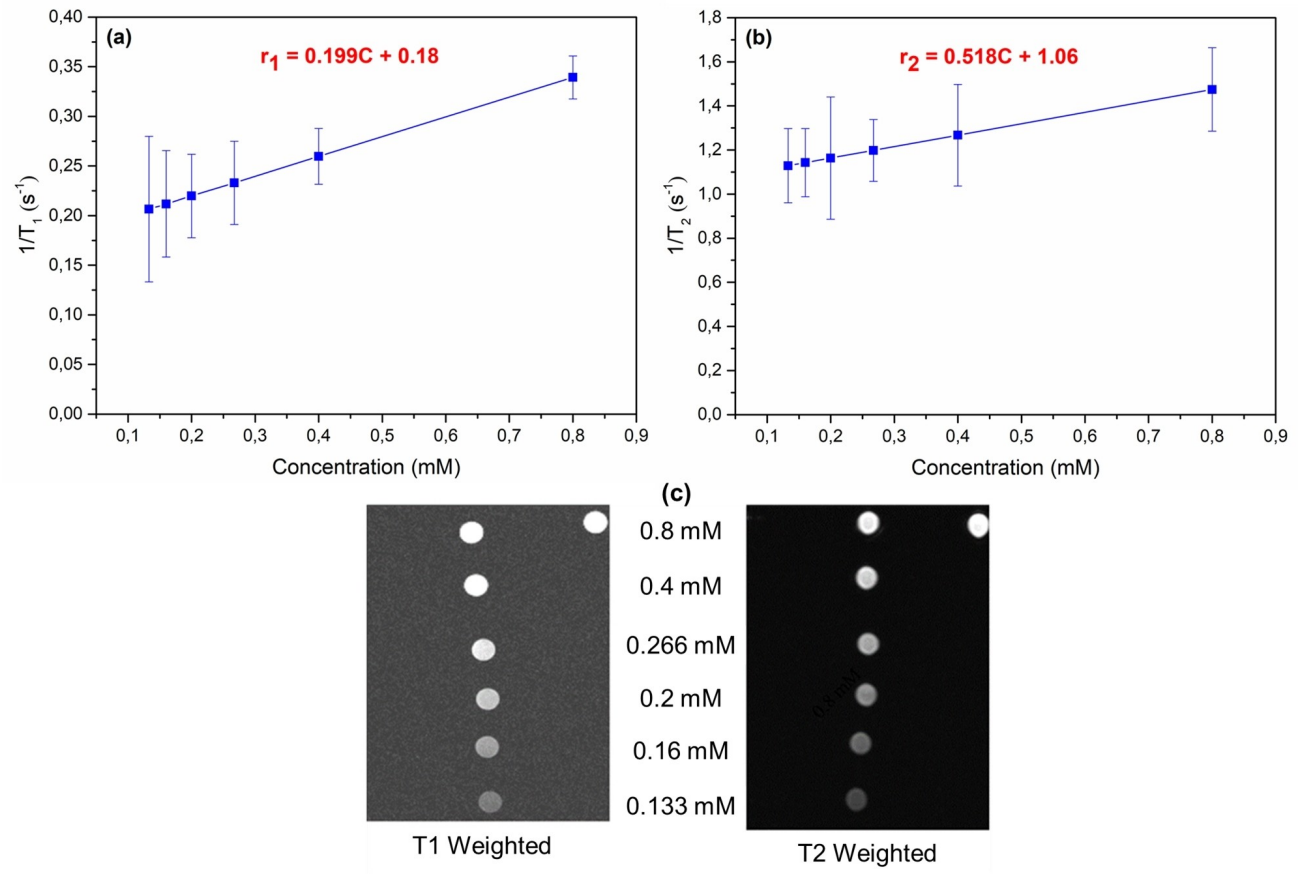

Figure 6. MRI Relaxivity Measurements at 3T: (a) For T1 mapping: 13 different TI values: [24 100 200 400 600 700 750 800 900 1000 1250 1500 1900] ms TR = 2000 ms, TE = 12 ms, Slice thickness = 4 mm, FOV = 101 mm × 144 mm, Resolution = 0.56 mm × 0.56 mm (b) For T2 mapping: 16 different TE values: [10 15 20 40 50 60 80 100 150 200 250 300 400 600 800 1000] ms TR = 3000 ms, Slice thickness = 4 mm, FOV = 114 mm × 144 mm, Resolution = 0.56 mm × 0.56 mm.

Conclusions

Within the scope of the study, iron oxide shell and yolk shell formation were provided so that quantum dots could be used as MRI agents. therefore, MRI contrast agent with superior properties was synthesized. In the presence of Yolk-shell CdSe/ZnS@Fe_2O_3 nanoparticles, $Fe(CO)_5$ and OAm, synthesis sonochemical synthesis method was used to eliminate the disadvantage of low photoluminescence quantum yield caused by high temperature. The sonochemical synthesis method of magnetic fluorescent NPs, which can be used as MRI contrast agents, has allowed the formation of nanomaterials with improved quantum efficiency and homogeneous size distributions. Maximum photoluminescence quantum yields of magnetic fluorescent NPs were achieved at 60 °C injection temperature of $Fe(CO)_5$, $Fe(CO)_5$/CdSe@ZnS ratio 0.7, OAm/$Fe(CO)_5$ volume ratio 1.43, oxidation time 5 min and 80% sonication speed. Under these conditions, the iron oxide shell on its surface was supported by XPS analysis. In addition, the thickness of this shell was determined to be around 2.5 nm in the dimensional analysis. MRI analysis demonstrated the possibility of using these particles as MRI positive contrast agents. These optically active magnetic nanoparticles would pave the way for the future of the advanced bio-imaging systems.

Supporting Information Summary

Effect of sonication rate and oxidation time on magnetic particle sizes and photoluminescence quantum yields and experimental section on the synthesis of nanoparticles can be found in Supporting Information.

Acknowledgements

EM acknowledges TUBITAK 20AG026 project and partial support from the Turkish Academy of Sciences Distinguished Young Scientist Award (TUBA-GEBIP).

Conflict of Interest

The authors declare no conflict of interest.

Data Availability Statement

Research data are not shared.

Keywords: Imaging agents · Magnetic fluorescent nanoparticles · MRI contrast agents · Quantum dots · Sonochemical decomposition · Yolk-shell CdSe/ZnS@Fe_2O_3

[1] M. Bloemen, D. Debruyne, P. Demeyer, K. Clays, A. Gils, N. Geukens, C. Bartic, T. Verbiesta, *RSC Adv.* **2014**, *4*, 10208–10211.
[2] Q. Mu, H. Xu, Y. Li, S. Ma, *The Analyst* **2013**, *139*, 93–98.
[3] Y. A. Chen, K. H. Chou, Y. Y. Kuo, C. Y. Wu, P. W. Hsiao, P. W. Chen, S. H. Yuan, D. S. Wuu, *Nanomaterials* **2019**, *999*, 7–9.
[4] J. Zylstra, J. Amey, N. J. Miska, L. Pang, C. R. Hine, J. Langer, R. P. Doyle, M. M. A. Maye, *Langmuir* **2011**, *27*, 4371–4379.
[5] J. Li, M. Mao, F. Wu, Q. Li, L. Wei, L. Ma, *Anal. Methods* **2018**, *10*, 29.
[6] S. Mourdikoudis, L. M. Liz-Marzá, *Chem. Mater.* **2013**, *25*, 9, 1465–1476.
[7] A. Heuer-Jungemann, N. Feliu, I. Bakaimi, M. Hamaly, A. Alkilany, I. Chakraborty, A. Masood, M. F. Casula, A. Kostopoulou, E. Oh, K. Susumu, M. H. Stewart, I. L. Medintz, E. Stratakis, W. J. Parak, A. G. Kanaras, *Chem. Rev.* **2019**, *119*, 8, 4819–4880.
[8] G. Kremser, T. Rath, B. Kunert, M. Edler, G. Fritz-Popovski, R. Resel, I. Letofsky-Papst, W. Grogger, G. J. Trimmel, *Colloid Interface Sci.* **2012**, *369*, 154–15.
[9] K. C. Leung, S. Xuan, X. Zhu, D. Wang, C. P. Chak, S. F. Lee, W. K. W. Ho, B. C. T. Chung, *Chem. Soc. Rev.* **2012**, *41*, 1911–1928.
[10] F. Lin, W. Chen, Y. Liao, R. Doong, Y. Li, *Nano Res.* **2011**, *4*, 1223–1232.
[11] J. P. Mehta, B. R. Knappett, G. Divitini, E. Ringe, P. A. Midgley, D. Fairen-Jimenez, A. E. H. Wheatley, *Part. Part. Syst. Charact.* **2018**, *35*, 1800120.
[12] S. Caspani, R. Magalhães, J. P. Araújo, C. T. Sousa, *Materials* **2020**, *13*, 2586.
[13] M. Imran, A. M. Affandi, M. M. Alam, A. Khan, A. I. Khan, *Nanotechnology* **2021**, *32*, 422001.
[14] M. Imran, A. H. Shaik, A. R. Ansari, A. Aziz, S. Hussain, A. F. F. Abouatiaa, A. Khan, M. R. Chandan, *RSC Adv.* **2018**, *8*, 13970–13975.
[15] M. Imran, A. R. Ansari, A. H. Shaik, A. Aziz, S. Hussain, A. Khan, M. R. Chandan, *Mater. Res. Express* **2018**. *5*, 3.
[16] M. Imran, M. M. Alam, S. Hussain, A. Abutaleb, A. Aziz, M. R. Chandan, K. Irshad, A. M. A. Al-Hagri, O. Y. Bakather, A. Khan, *Eur. Phys. J. Plus* **2021**, *136*, 752.
[17] M. Z. Iqbal, X. Ma, T. Chen, L. Zhang, W. Ren, L. Xiang, A. J. Wu, *Mater. Chem. B* **2015**, *3*, 5172–5181.
[18] H. N. Lari, D. Farhanian, D. C. Boffito, G. S. Patience, G. Crescenzo, J. Chaouki, J. R. Tavares, *Catal. Commun.* **2017**, *100*, 19–23.
[19] H. Kura, M. Takahashi, T. Ogawa, *J. Phys. Chem. C* **2010**, *114*, 5835–5838.
[20] M. Kim, H. Song, *J. Mater. Chem. C* **2014**, *2*, 4997–5004.
[21] B. Quan, X. Liang, G. J. Orcid, J. Ma, P. Ouyang, H. Gong, G. Xu, Y. Du, *ACS Appl. Mater. Interfaces* **2017**, *9*, 9964–9974.
[22] G. Sun, W. Xing, R. Xing, L. Cong, S. Tong, S. Yu, *Oncol. Lett.* **2018**, *15*, 2471–2476.
[23] X. Sun, R. Dai, J. Chen, W. Zhou, T. Wang, A. R. Kost, C. K. Tsung, Z. An, *Opt. Express* **2014**, *22*, 519–524.
[24] O. Chen, L. Riedemann, F. Etoc, H. Herrmann, M. Coppey, M. Barch, C. T. Farrar, J. Zhao, O. T. Bruns, H. Wei, P. Guo, J. Cui, R. Jensen, Y. Chen, D. K. Harris, J. M. Cordero, Z. Wang, A. Jasanoff, D. Fukumura, R. Reimer, M. Dahan, R. K. Jain, M. G. Bawendi, *Nat. Commun.* **2014**, *5093*, 1–8.
[25] A. Feld, J. P. Merkl, H. Kloust, S. Flessau, C. Schmidtke, C. Wolter, J. Ostermann, M. Kampferbeck, R. Eggers, A. Mews, T. Schotten, H. Weller, *Angew. Chem., Int. Ed.* **2015**, *54*, 12468–12471.
[26] S. K. Pahari, S. Olszakier, I. Kahn, L. Amirav, *Chem. Mater.* **2018**, *30*, 775–780.
[27] M. Reaz, A. Haque, D. M. Cornelison, A. Wanekaya, R. Delong, K. Ghosh, *Physica E* **2020**, *123*, 114090.
[28] J. Hao, H. Liu, J. Miao, R. Lu, Z. Zhou, B. Zhao, B. Xie, J. Cheng, K. Wang, M. H. Delville, *Sci. Rep.* **2019**, *9*, 12048.
[29] Y. Xıao, R. Paudel, J. Lıu, C. Ma, Z. Zhang, S. Zhou, *Int. J. Mol. Med.* **2016**, *38*, 1319–1326.
[30] G. Azizian, N. Riyahi-Alam, S. Haghgoo, H. R. Moghimi, R. Zohdiaghdam, B. Rafiei, E. Gorji, *Nanoscale Res. Lett.* **2012**, *7*, 549.
[31] M. A. Fortin, R. M. Petoral, F. Söderlind, A. Klasson, M. Engström, T. Veres, P. O. Kall, K. Uvdal, *Nanotechnology* **2007**, *18*, 395501–395510.

Submitted: January 16, 2022
Accepted: June 9, 2022